Appl Phys A (2013) 112:623–629
DOI 10.1007/s00339-013-7836-7

Applied Physics A
Materials Science & Processing

RAPID COMMUNICATION

Influence of ambient pressure on the hole formation in laser deep drilling

S. Döring · S. Richter · F. Heisler · T. Ullsperger · A. Tünnermann · S. Nolte

Received: 14 June 2013 / Accepted: 28 June 2013 / Published online: 9 July 2013

Abstract We investigate the temporal evolution of the hole depth and shape for percussion drilling at different ambient pressure conditions. Deep drilling is performed in silicon as target material by ultrashort laser pulses at 1030 nm and a duration of 8 ps. Simultaneously, the backlit silhouette of the hole is imaged perpendicular to the drilling direction. While typical process phases like depth development and shape evolution are very similar for atmospheric pressure down to vacuum conditions (10^{-2} mbar), the ablation rate in the initial process phase is significantly increased for reduced pressure. The number of pulses till the stop of the drilling process also increases by a pressure reduction and exceeds drilling at atmospheric conditions by two orders of magnitude for a pressure of ca. 10^{-2} mbar. Accordingly, the maximum achievable hole depth is more than doubled. We attribute this behavior to an enlarged mean free path for ablation products at reduced pressure and therefore lower or no deposition of particles inside the hole capillary under vacuum conditions while debris fills the hole already after a few thousand pulses at atmospheric pressure. This is supported by scanning electron cross section images of the holes.

S. Döring (✉) · S. Richter · F. Heisler · T. Ullsperger · A. Tünnermann · S. Nolte
Institute of Applied Physics, Abbe Center of Photonics, Friedrich–Schiller-Universität Jena, Max–Wien-Platz 1, 07743 Jena, Germany
e-mail: sven.doering@uni-jena.de

A. Tünnermann · S. Nolte
Fraunhofer Institute for Applied Optics and Precision Engineering, Albert–Einstein-Straße 7, 07745 Jena, Germany

1 Introduction

Ultrashort laser pulses with their specific ablation characteristics, like nearly direct solid-vapor transition and negligible thermal impact, offer a lot of advantages for the fabrication of high quality microstructures [1–5].

For the generation of deep structures with high aspect ratio, especially holes, additional challenges are encountered, including e.g. the decrease of ablation rate with increasing depth until the complete stop of ablation as well as the change in the shape of the ablated structure which is no longer solely determined by the incident laser beam. Previous investigations of the hole formation in silicon revealed three distinct process phases [6, 7]. After the excavation of an ideally shaped capillary during the first 100 to 200 pulses, the hole shape is subject to the formation of imperfections like indents on the side walls, bulges, branches and even several tips. This phase can continue for several thousand pulses depending on the applied pulse energy. Afterwards, in the final third phase, ablation only takes place on the side walls while the depth remains constant. The formation of the imperfections might be caused by scattering or deflection of the incoming pulse by ablation products that are deposited within the hole capillary. The deposits arise from the accumulation of atoms, ions and clusters or nanoparticles with a size of a few nanometers that are generated during material ablation by ultrashort laser pulses with a typical pulse duration <10 ps [8–10]. The deposition and aggregation of the ablation particles is essentially influenced by the ambient pressure. For ablation of silicon, cotton like aggregations of particles on the surface in the vicinity of ablation structures were observed at atmospheric pressure (1000 mbar), while a reduced density of debris or even no particles were found for lower pressure (10^{-1} mbar) [11]. For very high fluences, a significant amount of melt is generated even for ultrashort

pulses and the formation of a layer of molten material as well as the ejection of melt droplets may have to be considered [12]. Furthermore, it has been shown that a reduction of the ambient pressure leads to an increase in drilling efficiency. Ablation rate measurements on stainless steel and aluminum in the ps- and fs-regime revealed an increase of the average ablation depth per pulse of about 30–50 % for fluences in the order of 10 J/cm^2 when the ambient pressure is reduced to 100 mbar or less [13–15]. Similar results have also been obtained for drilling with nanosecond pulses [16]. Moreover, this effect can be accompanied by a decrease of the hole diameter [13].

The effect of the pressure conditions on the drilling process and resulting hole geometry needs further systematic investigation. In this work, we specifically analyze the influence of the ambient pressure on the drilling behavior. In particular, we study the complete hole shape formation to characterize the drilling process under different ambient pressures from atmospheric conditions (approx. 1000 mbar) to medium vacuum ($<10^{-2}$ mbar). The role of the redeposition of ablation particles is evaluated by taking scanning electron microscope images of hole cross sections.

2 Experimental setup

For investigating the drilling process for different pressure conditions, the silicon sample is placed inside a vacuum chamber which allows to control the ambient pressure by use of a vacuum pump and needle valve from about 1000 mbar (atmospheric conditions) to approximately $2 \cdot 10^{-3}$ mbar (medium vacuum). The actual pressure is measured by a combined Pirani and ion gauge (ATMION Wide Range Manometer). The drilling laser (Trumpf TruMicro 5050), operating at a wavelength of 1030 nm and a pulse duration of 8 ps (FWHM), is focused onto the sample surface by a plano-convex lens with a focal length of 100 mm, which is typical for micromaching applications. We used pulse energies form 25 µJ to 125 µJ, corresponding to an applied fluence of 8 J/cm^2 to 40 J/cm^2 in the focus. During the drilling process, the focus position is not moved, which means percussion drilling is performed. A second laser at 1060 nm is used to illuminate the sample perpendicular to the drilling direction and project the evolving silhouette of the hole onto a CCD-camera. The imaging setup is adapted from previous investigations, see [6]. The samples are prime grade crystalline silicon wafers with n-doping (resistivity $<10\ \Omega\,$cm) and ⟨100⟩ orientation perpendicular to the drilling direction. Nevertheless, our preliminary investigations showed no influence of the crystal orientation on the drilling results.

The mean free path Λ for gas molecules at a pressure p can be estimated by the model of an ideal gas [17] to be

$$\Lambda = \frac{kT}{\sqrt{2}\pi\, d^2 p} \tag{1}$$

Table 1 Pressure and corresponding mean free path for nitrogen at room temperature

p	Λ
1000 mbar	95 nm
100 mbar	950 nm
1 mbar	95 µm
10^{-2} mbar	9.5 mm

and is therefore inversely proportional to the pressure. Here, k denotes the Boltzmann constant, T the temperature and d the diameter of the gas molecules. Table 1 gives an overview of the pressures used in the experiments and the corresponding mean free path for nitrogen molecules with $d \approx 0.31$ nm [18] at room temperature.

This yields a rough approximation of the movability of the ablation products, since the ambient gas will offer a certain mechanical resistance against their expansion. The actual mean free path of the ablated particles can differ from the values in Table 1 as they differ in size, especially nanoparticles/clusters, but also have a higher temperature and directed movement away from the ablated surface. Nevertheless, within the pressure range examined in this experiment, we expect to increase the movability of the ablation products in such a way that it matches or even exceeds the hole depth up to several hundred micrometer.

In order to reveal the actual inner structure of the holes, we cleave the samples along the drilling direction. To facilitate this process, laser-structured grooves are added to the side walls of the sample before drilling. Afterwards, we carefully bend the sample perpendicular to those grooves, which leads to a fracture splitting the laser drilled hole. Since this technique does not involve any cutting or polishing steps, the particles which are deposited inside the hole capillary, are not moved or altered considerably by the cleaving and can be observed directly.

3 Results

The initial phase, which enfolds within the first few hundred pulses, shows the highest ablation rate of the drilling process. The end of this phase is marked by a significant drop in ablation rate. The development of the hole depth is shown in Fig. 1 for the first 800 pulses, for a pulse energy of 125 µJ and fluence of ca. 40 J/cm^2, respectively. For all pressure conditions, we observe an almost linear depth increase up to approximately 250 pulses, marked by the dashed line in Fig. 1. The average ablation rate during this initial phase is ca. 0.6 µm per pulse at standard atmospheric pressure. This rate is enhanced by approximately 40 % to 0.8 µm per pulse when the ambient pressure is reduced to 100 mbar. For further pressure reduction, the drilling rate does not exceed 0.8 µm per pulse, but stays constant at this level. This observation is in good agreement with ablation rate measurements

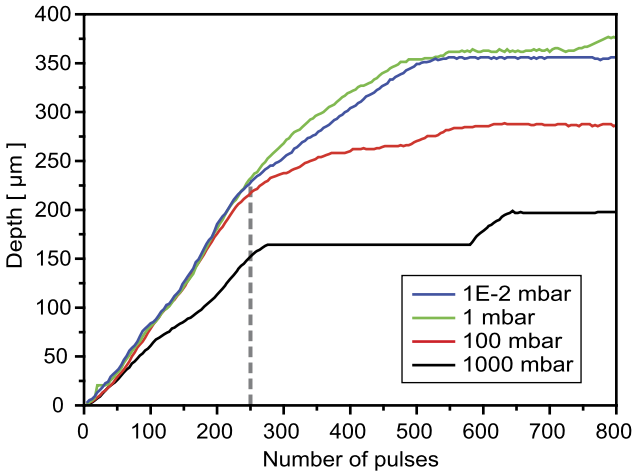

Fig. 1 Evolution of the hole depth as a function of number of pulses for a pulse energy of 125 µJ at different ambient pressures

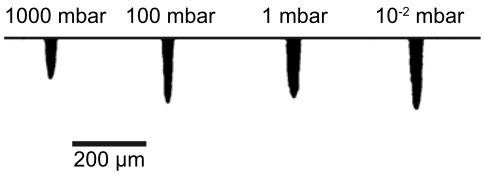

Fig. 2 The hole shape in the initial phase, here after $N = 200$ pulses for a pulse energy of 125 µJ, is similar for all ambient conditions and only differs in the achieved depth due to the higher ablation rate at reduced pressure

in stainless steel [13, 14] and aluminum [15], which show a similar increase in ablation rate for reducing the ambient pressure to 100 mbar and hold this level for further pressure reduction.

We attribute the higher ablation rate to a lower mechanical confinement of the ablation products and plume due to the surrounding gas envelope and less cooling when the ambient pressure is reduced, as proposed in [19]. The pressure dependence is also predicted by the thermal evaporation model, developed in [14]. A reduction of the confinement and of the laser induced shock wave, especially for pressures below 70 mbar, has also been observed by time-resolved shadowgraphy [20].

Figure 2 shows a comparison of the hole shape after 200 pulses, i.e. roughly at the end of the initial phase, for different pressure conditions. The holes drilled at reduced pressure exhibit a larger depth, but apart from that all holes have a similar shape and also similar width with a tapered upper part and a semicircular tip. This is the optimal hole shape for percussion drilling with a Gaussian shaped beam. In contrast to the investigations in [13], we do not observe a decrease of the entrance diameter of the holes with decreasing pressure at this early stage of the process.

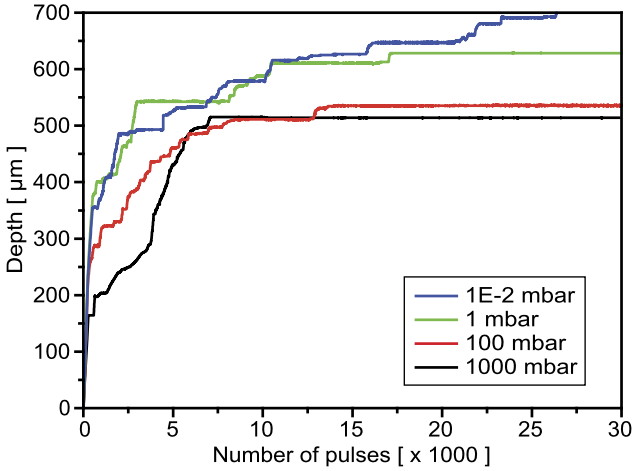

Fig. 3 The typical drilling behavior in the second drilling phase, here for a pulse energy of 125 µJ, is similar for all ambient pressure conditions. Especially the stepwise growth can be observed in every case

It is important to note that the increase in ablation rate in the initial phase at reduced ambient pressure, can be observed for all pulse energies under investigation here, i.e. from 25 µJ to 125 µJ. However, the effect is less noticeable for lower pulse energies. For example at a pulse energy of 50 µJ, the ablation rate increases only by ca. 25 % from 0.30 µm per pulse at 1000 mbar to 0.38 µm per pulse at 100 mbar or below. Investigations of the average drilling rate of metals under vacuum conditions observed a similar dependence on pulse energy and fluence, respectively [13, 15].

The following second phase of the drilling process features the formation of imperfections along the side walls of the hole, especially the formation of bulges and indents as well as a change of the drilling direction and the possible formation of multiple hole ends. This behavior is accompanied by periods of predominant transversal growth and a complete intermediate stop of forward drilling, which leads to a stepwise increase in the hole depth. In addition, the depth and shape evolution features significant statistical variations in this second drilling phase, especially with respect to occurrence and duration of the intermediate stop periods, see also previous investigations in [7]. We observe this typical behavior for all pressure conditions in our experiments. Figure 3 shows the hole depth evolution for a pulse energy of 125 µJ up to $N = 30{,}000$ pulses, covering this second drilling phase.

Due to the strong variations in depth increase, the exact hole depth at a certain time cannot be predicted and there is no longer such a clear dependence between depth and ambient pressure as has been in the initial phase. Despite these variations, the obtained statements for the drilling behavior and depth relations are nevertheless significant. While there are situations when the actual depth increases with decreasing pressure, e.g. in the range of 2,000 to 3,000 pulses, this

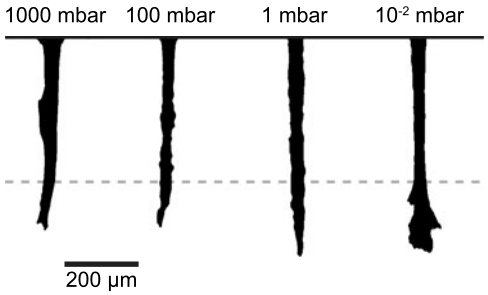

Fig. 4 Hole shape in the second drilling phase, after 10,000 pulses, for a pulse energy of 125 µJ

order of depth in dependence of the pressure can change due to the intermediate periods without forward drilling, compare e.g. to the range of around 5,000 to 10,000 pulses in Fig. 3, when drilling at 1000 mbar achieved a larger depth than drilling at 100 mbar and likewise for 1 mbar compared to 10^{-2} mbar. However, the maximum hole depth that is finally obtained increases with decreasing pressure, see e.g. Fig. 3 for more than 20,000 pulses and also the explanations below.

The hole shape in the second drilling phase, as depicted for a pulse energy of 125 µJ after 10,000 pulses in Fig. 4, shows the typical formation of indents on the side walls and bulges in the upper part of the hole for an ambient pressure of 1000 mbar. For lower pressures, these imperfections become smaller, but occur more frequent, see for example the holes obtained for pressures down to 1 mbar. The hole drilled at 10^{-2} mbar is almost free of imperfections along the upper part. Nevertheless, bending of the hole is present for all pressure conditions and occurs approximately at the same depth, marked by a dashed line in Fig. 4. In case of 10^{-2} mbar several bendings in different directions already occurred at this stage, which results in a dominant branching of the lower hole part. In addition, we observe a larger hole entrance diameter for atmospheric pressure than under vacuum conditions, which can be attributed to a nonlinear interaction of the ultrashort laser pulses with the ambient gas and a resulting beam broadening in agreement with the observations in [2, 21]. Nevertheless, in our observations this effect is limited to the hole entrance (position of the beam focus) and does not affect the entire depth.

In summary we observe a similar behavior and variation in depth evolution for different ambient pressure conditions. Also special hole shape features, like bending of the hole, are present for all pressure conditions in the second phase of the drilling process. On the other hand, the occurrence of bulges and indents on the side walls is reduced for drilling at lower ambient pressure.

To investigate the role of debris and particle redeposition on the drilling behavior, we directly examined the interior of the holes, by preparing high resolution cross section images, as described in Sect. 2. In Fig. 5 the respective images of holes drilled at standard atmospheric pressure $p = 1000$ mbar and vacuum at $p = 10^{-2}$ mbar after $N = 10{,}000$ pulses for a pulse energy of 125 µJ are shown for comparison.

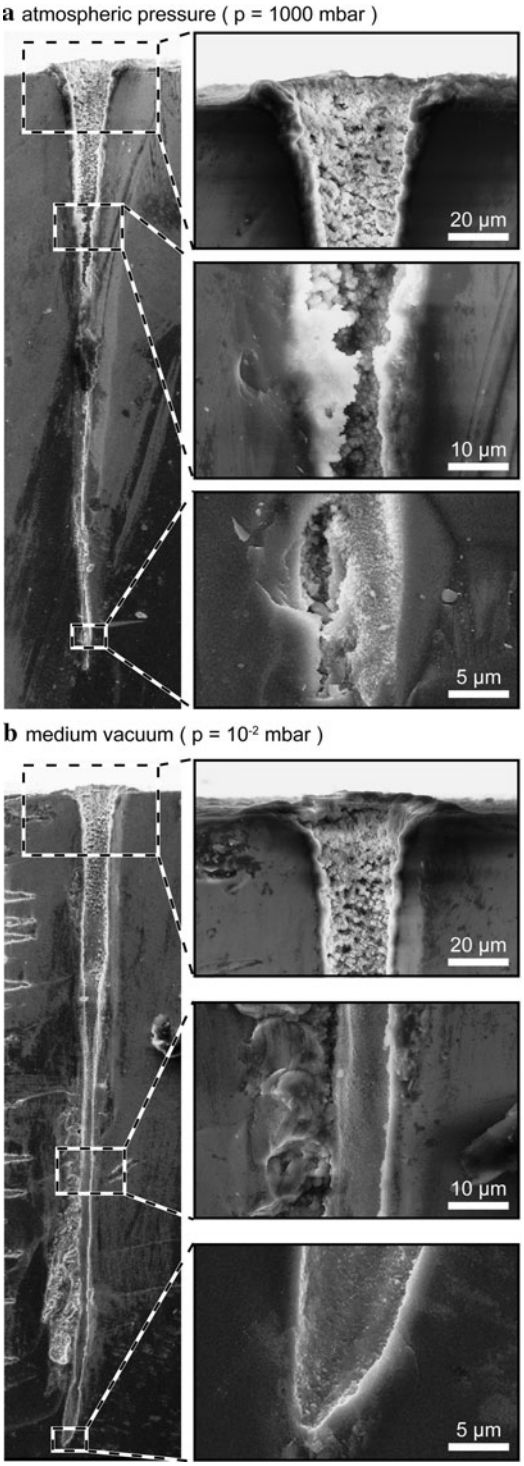

Fig. 5 Comparison of the interior of percussion drilled holes in silicon, after 10,000 pulses for a pulse energy of 125 µJ at a pressure of 1000 mbar (**a**) and 10^{-2} mbar (**b**)

For a pressure of 1000 mbar, see Fig. 5(a), a thick layer of agglomerated particles is forming a cloud or cotton like structure of particle clusters at the entrance of the hole. This layer also covers the inner side walls in the middle of the hole with similar thickness, density and structure. These debris structures extend far into the inside of the hole, which means they are stable against subsequent pulses. Hence, passing pulse flanks only lead to a low removal rate of those particles due to the large surface (caused by the roughness of the structures) and/or the occurring removal is leveled out by the redeposition of freshly ablated particles. Even at the tip of the hole, the side walls are covered with small particles and particle agglomerations. For a pressure of 10^{-2} mbar, see Fig. 5(b), the same thick particle layer is visible at the hole entrance, very similar to the situation at $p = 1000$ mbar. However, in contrast to higher pressure, the particle debris at the side walls decreases with increasing hole depth and already almost no particle deposition is observable in the middle of the hole, resulting in a clean hole capillary. Even at the hole tip, no redeposition of ablation particles is visible. Furthermore, the cross section features the typical bending and bulge formation, especially in the lower part of the hole, although no debris is present.

The particle agglomerations, which build up at atmospheric pressure, effectively reduce the open hole diameter, which leads to strong scattering of subsequent pulses propagating down the hole capillary. In the case of vacuum (10^{-2} mbar), a redeposition of ablation particles only takes place at the topmost part of the hole. Here, scattering is limited due to the large overall diameter of the hole. More important are the clear side walls in the middle and lower part of the hole, which show nearly no debris and therefore do not obstruct the pulse propagation.

Figure 6 shows the complete depth evolution for a pulse energy of 125 µJ over a range of 800,000 pulses for all pressure conditions. At high pressure, $p > 1$ mbar, the final depth is already reached after some thousand pulses, see also Table 2. The situation changes dramatically, if the pressure is decreased to 10^{-2} mbar. Drilling at medium vacuum, $p = 10^{-2}$ mbar, continues for the complete time under investigation, i.e. for about 800,000 pulses, which is about two orders of magnitude more than for atmospheric conditions. In this case, also the typical behavior of stepwise depth increase is most distinct. Notably, the intermediate periods of constant depth can last for more than 100,000 pulses and alternate with comparably short periods of depth increase of a few hundred to a few thousand pulses. As a general trend, the average ablation rate during the periods of depth increase decreases from step to step. At an early stage in this second phase at a few thousand pulses, the average drilling rate in one step is about 0.3 µm per pulse, comparable to the rate observed for higher pressures up to 1000 mbar at this pulse number. For deeper holes and at a later stage of the process,

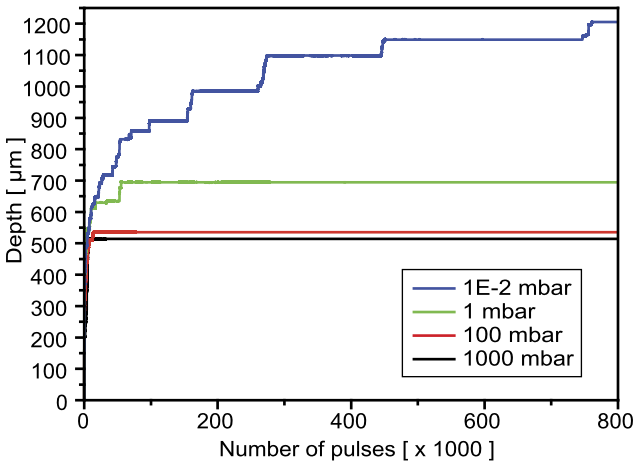

Fig. 6 The depth evolution continues for a higher number of pulses and reaches a larger final depth with decreasing ambient pressure, which is especially distinct for a pressure of 10^{-2} mbar. In this case, the typical stepwise increase in hole depth is most pronounced, too. (Here for a pulse energy of 125 µJ)

Table 2 The finally achievable hole depth d_{final} increases for reduced pressure in combination with the total number of pulses to reach this final depth N_{final}

p	50 µJ		125 µJ	
	d_{final}	N_{final}	d_{final}	N_{final}
1000 mbar	318 µm	4,500	515 µm	7,000
100 mbar	330 µm	5,500	535 µm	14,000
1 mbar	362 µm	7,500	685 µm	55,000
10^{-2} mbar	507 µm	45,000	>1200 µm	>800,000

the average rate is reduced to about 0.1 µm per pulse at approximately 16,000 pulses and merely 0.02 µm per pulse at around 450,000 pulses. Associated with the extended processing time, the finally obtained hole depth at 10^{-2} mbar reaches more than 1 mm and is more than 100 % larger compared to low vacuum or atmospheric pressure. This is only possible due to the significant decrease of particle deposition when the ambient pressure is reduced. Nevertheless, debris will also occur inside the capillary when a sufficient depth is reached, which will eventually be the case when the hole depth exceeds the estimated mean free path of the particles, which is already indicated by the particle depositions at the hole entrance after 10,000 pulses in Fig. 5. Hence, the same obstruction of the pulse propagation inside the hole will occur for vacuum conditions as in case of atmospheric pressure and prevent further ablation and forward drilling at the tip of the hole.

Table 2 summarizes the finally achieved depth d_{final} and the number of pulses N_{final} that contribute to forward drilling until this maximum depth is reached for pulse energies of 50 µJ and 125 µJ for the different pressure condi-

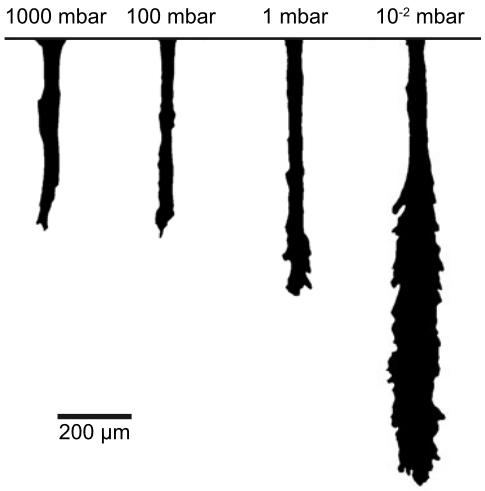

Fig. 7 The final hole shape shows a pronounced branching in the part of extended depth for a pressure of 1 mbar and especially 10^{-2} mbar compared to higher ambient pressure, here for a pulse energy of 125 µJ

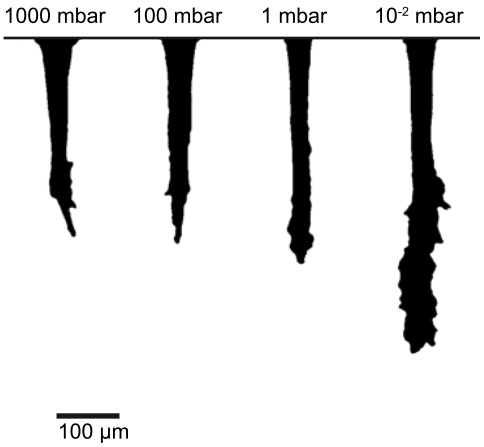

Fig. 8 Continuous bending and branching of the lower hole part occurs at reduced ambient pressure, especially 10^{-2} mbar compared to atmospheric conditions, here for a pulse energy of 50 µJ

tions under investigation. Again, the effect of reduced ambient pressure is less pronounced for lower pulse energies, but still significant. For a pulse energy of 50 µJ, the number of pulses to reach the final depth increases by one order of magnitude, from 4,500 at 1000 mbar to 45,000 at 10^{-2} mbar in combination with an increase of the final depth of ca. 60 %.

The final shape of the holes at the end of the drilling process is shown in Fig. 7 for a pulse energy of 125 µJ.

The shape that has formed for 1000 mbar and 100 mbar is very similar and shows only one bending of the hole. For a pressure of 1 mbar, several bendings of the hole occurred, resulting in a highly branched lower part of the hole, similar to a crown like structure. This is comparable to the state that was reached already after 10,000 pulses for 10^{-2} mbar, see Fig. 4, which means this development already sets in at a lower number of pulses when the ambient pressure is reduced further. For 10^{-2} mbar, the complete lower half of the hole consists of a multitude of branches and resembles a narrow tree. Our in-situ observations show that each of the tips that are visible in the final state were formed individually and consecutively during the drilling process. Therefore, each branch is formed by one bending of the hole and ablation only takes place in one direction at a time. Furthermore, we also observed the formation of branches in the middle section of the hole during the intermediate periods of constant depth, which means that additional branches also formed in parts that already bear sideward channels. Please keep in mind that Fig. 7 only shows the hole's silhouette. Therefore, the three dimensional character of the hole shape and the individual branches cannot be visualized correctly and it seems like the hole consists of a large internal cavity in the lower part, which is not necessarily the case. Remarkably, the uttermost tips of the branches all have approximately the same distance from the center axis of the hole capillary.

This effect of the pressure conditions on the hole shape occurs in the same way also for lower incident pulse energy, see for example $E_P = 50$ µJ in Fig. 8. Nevertheless, due to the lower pulse energy compared to Fig. 7, the effect is less prominent.

4 Discussion

Our investigations of the hole formation process for different ambient pressure conditions show a similar drilling behavior with respect to the occurrence of the three typical process phases and the depth evolution. However, a reduced ambient pressure leads to an increased ablation rate and drilling efficiency during the first process phase, which is about 40 % for a pressure reduction from atmospheric conditions (1000 mbar) to medium vacuum (10^{-2} mbar) at 125 µJ pulse energy. The influence of the pressure in the first process phase becomes more distinct for higher incident pulse energies. We attribute the increase in ablation rate to a lower mechanical confinement of ablated particles, plume and the laser generated shock-wave by the ambient gas at reduced pressure is reduced, in accordance with [14, 19, 20].

For deep drilling, the ambient pressure significantly effects the flow and deposition of ablation particles in the enclosed environment of the hole capillary. In the case of atmospheric pressure the estimated mean free path of these particles is in the sub-micrometer range and leads to a redeposition of particles even in the close vicinity of the ablation spot, i.e. the tip of the hole. For continuous drilling, the filling of the hole capillary with debris and the resulting obstruction and scattering of the pulse during propagation plays an important role for the early stop of the drilling process. In the case of vacuum ($p = 10^{-2}$ mbar), the estimated

mean free path of the ablation products is in the order of several hundred micrometer or even millimeter (see Table 1). Therefore, the side walls in the middle and lower part of the hole show nearly no debris and hence no obstruction of the pulse during propagation. The filling of the hole capillary, as already indicated by particle depositions at the hole entrance even for 10^{-2} mbar in Fig. 5(b), is postponed by a reduced ambient pressure. Therefore, drilling under vacuum conditions does not stop after a few thousand pulses, but can continue for several hundred thousand pulses and achieve a final hole depth that is 100 % larger compared to high ambient pressure (for 125 µJ). Nevertheless, we observe the same hole formation characteristics, with a stepwise depth development which is subject to strong variations and the typical bending and bulge formation of the hole, for all pressure conditions. Hence, the particle deposition inside the hole does not primarily influence the principal drilling behavior and shape formation.

5 Conclusions and outlook

During the first process phase, a reduced ambient pressure leads to an increased ablation rate and drilling efficiency that is about 40 % for a pressure reduction from atmospheric conditions (1000 mbar) to medium vacuum (10^{-2} mbar) at 125 µJ pulse energy. In addition, the significantly reduced particle deposition under vacuum conditions leads to a substantially prolonged drilling process and accordingly larger depth. For a pulse energy of 125 µJ this results in two orders of magnitude more pulses till the stop of forward drilling and 100 % increased depth at 10^{-2} mbar compared to atmospheric pressure. These effects are more distinct for higher incident pulse energies. Nevertheless, deviations of the hole formation from the ideal shape, especially sideward bends and indents on the hole walls, occur likewise for high and low pressure conditions and also develop in the hole's complete lower part of extended depth at reduced ambient pressure.

To improve the hole quality, which essentially means a suppression of bendings and bulges, a spatial shaping of the laser beam might be useful in influencing the shape formation of the hole in order to keep a straight drilling for larger depths. Furthermore, an advanced management of the energy deposition in the material, for example by applying bursts of laser pulses, may positively affect the hole shape formation. However, the suggested approaches still require fundamental experimental and theoretical investigations in future studies.

Acknowledgements We acknowledge financial support by the Deutsche Forschungsgemeinschaft (DFG, Leibniz program) and the Fraunhofer–Gesellschaft. Sören Richter is supported by the Hans L. Merkle Stiftung.

References

1. F. Dausinger, F. Lichtner, H. Lubatschowski, *Femtosecond Technology for Technical and Medical Applications* (Springer, Berlin, 2004)
2. D. Breitling, A. Ruf, F. Dausinger, Proc. SPIE **5339**, 49 (2004)
3. S. Preuss, A. Demchuk, M. Stuke, Appl. Phys. A **61**, 33 (1995)
4. B.N. Chichkov, C. Momma, S. Nolte, F. von Alvensleben, A. Tünnermann, Appl. Phys. A **63**, 109 (1996)
5. S. Nolte, C. Momma, H. Jacobs, A. Tünnermann, B.N. Chichkov, B. Wellegehausen, H. Welling, J. Opt. Soc. Am. B **14**, 2716 (1997)
6. S. Döring, S. Richter, S. Nolte, A. Tünnermann, Opt. Express **18**, 20395 (2010)
7. S. Döring, S. Richter, S. Nolte, A. Tünnermann, Appl. Phys. A **105**, 69 (2011)
8. S. Amoruso, B. Toftmann, J. Schou, R. Velotta, X. Wang, Thin Solid Films **453–454**, 562 (2004)
9. A.V. Bulgakov, I. Ozerov, W. Marine, Thin Solid Films **453–454**, 557 (2004)
10. S. Amoruso, R. Bruzzese, C. Pagano, X. Wang, Appl. Phys. A **89**, 1017 (2007)
11. T. Matsumura, A. Kazama, T. Yagi, Appl. Phys. A **81**, 1393 (2005)
12. A. Michalowski, D. Walter, F. Dausinger, T. Graf, J. Laser Micro Nanoeng. **3**, 211 (2008)
13. C. Föhl, D. Breitling, F. Dausinger, Proc. SPIE **5121**, 271 (2003)
14. F.P. Mezzapesa, L.L. Columbo, M. Brambilla, M. Dabbicco, A. Ancona, T. Sibillano, G. Scamarcio, Appl. Phys. Lett. **101**, 011103 (2012)
15. A.E. Wynne, B.C. Stuart, Appl. Phys. A **76**, 373 (2003)
16. S.M. Klimentov, P.A. Pivovarov, V.I. Konov, D. Breitling, F. Dausinger, Quantum Electron. **34**, 537 (2004)
17. D. Meschede, *Gerthsen Physik*, 21st edn. (Springer, Berlin, 2002), pp. 221–223
18. A. Bondi, J. Phys. Chem. **68**, 441 (1964)
19. A. Di Bernardo, C. Courtois, B. Cros, G. Matthieussent, D. Batani, T. Desai, F. Strati, G. Lucchini, Laser Part. Beams **21**, 59 (2003)
20. Z. Wu, X. Zhu, N. Zhang, J. Appl. Phys. **109**, 053113 (2011)
21. S. Besner, J.-Y. Degorce, A.V. Kabashin, M. Meunier, Appl. Surf. Sci. **247**, 163 (2005)